



CHALMERS
UNIVERSITY OF TECHNOLOGY

Electro-Chemo-Mechanical Modeling of Artificial Solid Electrolyte Interphase to Enable Uniform Electrodeposition of Lithium Metal Anodes

Downloaded from: <https://research.chalmers.se>, 2024-03-13 10:55 UTC

Citation for the original published paper (version of record):

Liu, Y., Xu, X., Kapitanova, O. et al (2022). Electro-Chemo-Mechanical Modeling of Artificial Solid Electrolyte Interphase to Enable Uniform Electrodeposition of Lithium Metal Anodes. *Advanced Energy Materials*, 12(9).
<http://dx.doi.org/10.1002/aenm.202103589>

N.B. When citing this work, cite the original published paper.

Electro-Chemo-Mechanical Modeling of Artificial Solid Electrolyte Interphase to Enable Uniform Electrodeposition of Lithium Metal Anodes

Yangyang Liu, Xieyu Xu, Olesya O. Kapitanova, Pavel V. Evdokimov, Zhongxiao Song, Aleksandar Matic,* and Shizhao Xiong*

Nonuniform electrodeposition of lithium during charging processes is the key issue hindering development of rechargeable Li metal batteries. This deposition process is largely controlled by the solid electrolyte interphase (SEI) on the metal surface and the design of artificial SEIs is an essential pathway to regulate electrodeposition of Li. In this work, an electro-chemo-mechanical model is built and implemented in a phase-field modelling to understand the correlation between the physical properties of artificial SEIs and deposition of Li. The results show that improving ionic conductivity of the SEI above a critical level can mitigate stress concentration and preferred deposition of Li. In addition, the mechanical strength of the SEI is found to also mitigate non-uniform deposition and influence electrochemical kinetics, with a Young's modulus around 4.0 GPa being a threshold value for even deposition of Li. By comparison of the results to experimental results for artificial SEIs it is clear that the most important direction for future work is to improve the ionic conductivity without compromising mechanical strength. In addition, the findings and methodology presented here not only provide detailed guidelines for design of artificial SEI on Li-metal anodes but also pave the way to explore strategies for regulating deposition of other metal anodes.

cathode and anode materials need to be developed for next-generation batteries with a performance beyond current commercial lithium-ion batteries. Lithium (Li) metal, with a theoretical specific capacity of 3860 mAh g⁻¹ and low reduction potential of -3.04 V, is regarded as the ultimate high-energy-density anode material to replace graphite that is currently used in commercial Li-ion batteries, which has a much lower theoretical specific capacity (372 mAh g⁻¹).^[2] Unfortunately, the implementation of lithium metal batteries (LMBs) is hindered by the nonuniform electrodeposition of Li with uncontrollable formation of dendrites as well as side-reactions between Li and the electrolyte.^[3]


Understanding the electrodeposition behavior of Li is of primary importance for the implementation of LMBs, but it is also full of challenges as the process is controlled by an electro-chemo-mechanic (ECM) mechanism coupling the electrochemical reduction of Li-ion, mechanical stresses at the interface, and chemical reactions with the electrolyte.^[4] It has been previously reported that a high exchange current density on the Li-electrode combined with rapid depletion of Li-ions on the electrode surface, which is governed by electrolyte concentration, temperature as well as applied current density, by are two main

1. Introduction

Anxiety about the driving range of electric vehicles and endurance of portable devices is invariably accompanying their users in modern society because of limited energy-density of the battery.^[1] To overcome this issue, high-energy-density

Y. Liu, Z. Song
State Key Laboratory for Mechanical Behavior of Materials
Xi'an Jiaotong University
Xi'an 710049, P. R. China

X. Xu, O. O. Kapitanova, P. V. Evdokimov
Department of Materials Science
Lomonosov Moscow State University
Leninskie gory 1, Moscow 119991, Russia

 The ORCID identification number(s) for the author(s) of this article can be found under <https://doi.org/10.1002/aenm.202103589>.

© 2022 The Authors. Advanced Energy Materials published by Wiley-VCH GmbH. This is an open access article under the terms of the Creative Commons Attribution License, which permits use, distribution and reproduction in any medium, provided the original work is properly cited.

O. O. Kapitanova
Center for Photonics and 2D Materials
Moscow Institute of Physics and Technology
9 Institutskiy per., Dolgoprudny, Moscow Region 141701, Russia
P. V. Evdokimov
Kurnakov Institute of General and Inorganic Chemistry of the Russian Academy of Sciences
Leninskii prosp. 31, Moscow 119071, Russia
A. Matic, S. Xiong
Department of Physics
Chalmers University of Technology
Göteborg SE 412 96, Sweden
E-mail: matic@chalmers.se; shizhao.xiong@chalmers.se

DOI: 10.1002/aenm.202103589

underlying factors for dendritic electrodeposition.^[5] In addition, the solid electrolyte interphase (SEI), which is formed by the reaction between Li-metal and electrolyte, also plays a crucial role in the kinetics of the electrochemical deposition process.^[4a,6] The SEI film formed on the metal anode controls the charge-transfer and ion transport between the bulk electrode and the electrolyte close to the electrode surface.^[7] The mechanical property of the SEI is also of importance since it will undergo repeated interface displacement during Li electrochemical stripping and plating with a risk of crack formation or even breakage.^[8] As a result, fresh Li will be exposed to, and continuously react with, the electrolyte, leading to electrolyte consumption, loss of active Li, and accumulation of insulating by-products at the interface.^[9] This leads to lower Coulombic efficiency and ultimately causes failure of batteries.^[10] Therefore, the ionic conductivity and the mechanical strength of the SEI film are critical for the electrochemical performance of Li-metal anodes.

Many strategies have been developed to tune the properties of the SEI to suppress the formation of Li dendrites and enable uniform electrodeposition. Approaches to design the SEI layer on Li-metal anodes have been based on optimization of electrolyte formulation,^[11] physical vapor deposition,^[12] or in situ polymer coating,^[13] mainly aiming to improve ionic conductivity of the SEI to mitigate depletion of Li-ions at the Li-metal surface. There have also been efforts devoted to build artificial SEIs with enhanced mechanical properties to suppress its mechanical failure (breaking/cracking) caused by dendritic growth or interface displacement.^[14] However, an understanding of the relationship between properties of the SEI and the electrodeposition behavior of Li is still lacking due to the difficulty to simultaneously probe the influence of electrochemical and mechanical processes as well as to theoretically disentangle the contribution of these processes at the electrode/electrolyte interface. Several theories have been put forward to describe the electrochemical deposition process, including Butler–Volmer reaction kinetics representing local current distribution,^[15] space charge layer, and mass transfer limitations near the electrode surface.^[5b,16] From a mechanical point of view dendritic growth has been considered in relation to mean stress at plating/stripping and deformation of the SEI.^[15b,17] Specifically, the growth process of deposited Li has been proposed to be governed by elastic-plastic deformation of both Li metal and SEI,^[18] but so far little attention has been paid to thoroughly understand the ECM mechanism for deposition of Li in the presence of a SEI.

In this work, we build an electro-chemo-mechanical model involving electrochemical kinetics and mechanics to investigate how to tune the properties of an artificial SEI to enable uniform electrodeposition of Li. The model is developed from a modified Butler–Volmer equation including electric, stress and Li-ion concentration fields to describe the electrodeposition process at the interface between SEI and Li-metal. It is here implemented in a phase-field model with a structured substrate covered with an SEI. With this method, we disentangle the role of the ionic conductivity and Young's modulus of the SEI and show that both properties play significant roles in the electrodeposition behavior of Li. The results from the modeling are benchmarked with experimental data previously reported in literature and provide a guide to future design and optimization of artificial SEIs for Li metal anodes. The model and computing strategy

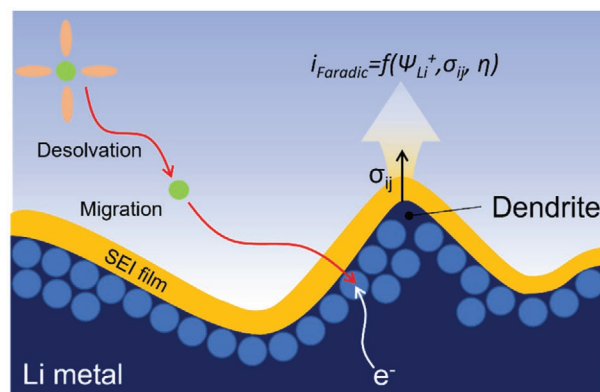


Figure 1. Schematic of electrodeposition of Li at the interface between the bulk metal electrode and SEI involving electrochemical kinetics of Li as well as mechanical stresses.

developed in this work are general and can readily be transferred to the design of protective interlayers for other metal anodes.^[19]

2. Results and Discussion

To investigate the electrodeposition of Li under coupled physical fields near the electrode surface, a structured substrate was built following the approach we previously reported and shown in Figure S1 (Supporting Information).^[5b] Usually the surface of Li metal should be flat after coating with artificial SEI, but the surface will not be perfectly flat during repeated plating/stripping and defects created during cycling will inevitably result in structural fluctuations.^[20] In this work, such structural fluctuations have been abstracted to a rectangularly patterned surface, with the substrate having rectangular pillars ($10 \times 5 \mu\text{m}$) and being covered by an artificial SEI film (uniform thickness of $1 \mu\text{m}$). This structure used in the electro-chemo-mechanical model is suitable to simulate the behavior of an artificial SEI since it can be considered as a homogeneous continuum in contrast to a native SEI.^[13] The detailed parameters for this electro-chem-mechanical model are summarized in Table S1 (Supporting Information). With phase-field modeling we can directly visualize the electric field, Li-ion concentration and the mechanical stresses at the interface and follow the evolution of the morphology of electrodeposited Li as a function of time. The simulations were run until either the gap between the pillars was closed, or as a result of a drastically decreased electrodeposition rate.

To simulate the electrodeposition process of Li from the electrolyte (**Figure 1**) a 2D transient model is used where the flux of Li ions is given by the Nernst-Planck equation:^[5b,16a,21]

$$\begin{cases} \bar{N}_e = -D_e \nabla c_e - q_{Li^+} u_e F c_e \nabla \phi_e \\ \bar{N}_s = -D_s \nabla c_s - q_{Li^+} u_s F c_s \nabla \phi_s \end{cases} \quad (1)$$

where \bar{N}_e and \bar{N}_s , D_e and D_s , c_e and c_s , u_e and u_s , ϕ_e and ϕ_s are the transfer vectors, the diffusion coefficients, the concentrations of Li ions, the ionic mobility, the potentials, in the electrolyte and in the SEI layer, respectively, and q_{Li^+} is the charge of the Li-ion and F is the Faraday constant.

The deposition process can be described according to the simplified reaction:^[22]



The local current density as a function of potential, Li-ion concentration and stress field can be expressed by a modified Butler-Volmer equation:^[23]

$$i = i_0 \exp\left(\frac{\alpha \Delta \mu_e}{RT}\right) \left[\exp\left(\frac{\alpha F}{RT} \eta\right) - \frac{c_{\text{Li}^+}}{c_{\text{Li}^+, \text{ref}}} \exp\left(-\frac{\beta F}{RT} \eta\right) \right] \quad (3)$$

where i_0 is the exchange current density, α , and β are the anodic and cathodic transfer coefficients, respectively, and $\alpha = \beta = \frac{1}{2}$ for a single-electron reaction. η is the overpotential that can be expressed as $\eta = (\phi_{\text{S},0} - \phi_e - \phi_s) - \Delta \phi_{\text{eq}}$, where $\phi_{\text{S},0}$ is the potential of the Li electrode. $c_{\text{Li}^+, \text{ref}}$ and c_{Li^+} are the Li-ion concentration in the electrolyte close to the substrate and in the SEI, respectively. The concentration of Li-ions near the substrate can be expressed as

$$c_{\text{Li}^+, \text{ref}}(0, t) = c_{\text{Li}^+} - \frac{2j\sqrt{t}}{F \sqrt{\frac{\pi q_{\text{Li}^+} c_{\text{Li}^+}}{\kappa_B T}} \psi} \quad (4)$$

after solving the mass conservation equation with related boundary conditions and applying the Nernst-Einstein equation.^[24,25] To describe the influence of a stress field on the local current density, the term $R = \exp\left(\frac{\alpha \Delta \mu_e}{RT}\right)$ is introduced in Equation (3) where the parameter $\Delta \mu_e$, defined as the electrochemical potential change induced by the local strain, includes hydrostatic stress ($\sigma_{kk} = \sigma_1 + \sigma_2 + \sigma_3$) as well as deviatoric stress (S_{ij}).^[26] Following the approach developed by Monroe and Newman, the deformation parameter $\Delta \mu_e$ can be expressed as:^[26b,27]

$$\Delta \mu_e(x) = -\frac{1}{2}(\bar{V}_{\text{Li}} + (1 - t_{\text{Li}^+})\bar{V}_{\text{LiX}}) \times \left\{ -\nabla_s \cdot \bar{n} \cdot \gamma - \bar{n} \cdot \left[S_{ij}^{\text{Li}} - S_{ij}^{\text{SEI}} \right] \right\} + \frac{1}{2}(\bar{V}_{\text{Li}} - (1 - t_{\text{Li}^+})\bar{V}_{\text{LiX}}) (\sigma_{kk}^{\text{Li}} + \sigma_{kk}^{\text{SEI}}) \quad (5)$$

where \bar{V}_{Li} and \bar{V}_{LiX} represent the partial molar volumes of Li metal and lithium salt, respectively, see Supporting information, t_{Li^+} is the transference number of Li-ions, γ and ∇_s are the surface energy and surface gradient, respectively. \bar{n} is the normal vector to the Li-metal/SEI interface. For a 2D calculation of electrodeposition, $-\nabla_s \cdot \bar{n}$ can be defined as the local curvature (K) of the displacement at Li-SEI interface^[26a,28] and assuming small strain at the interface, the kinematic stress-strain constitutive relation is given by Hooke's Law:^[29]

$$\sigma_{ij} = \frac{E}{1+\nu} \nabla \bar{\ell} + \frac{2\nu E}{1-2\nu} \quad (6)$$

where E is Young's modulus, $\bar{\ell}$ is the displacement of the Li-SEI interface and ν is Poisson's ratio, see details in Supporting Information. Substituting Equations (4), (5), and (6) into Equation (3), the local Faradic current density is now a

function of the ionic conductivity of the SEI, local stress, and the overpotential,

$$i_{\text{Faradic}} = f(\psi_{\text{Li}^+}, \sigma_{ij}, \eta) \quad (7)$$

To investigate role of ionic conductivity of the SEI on the electrodeposition of Li, the parameter Γ is introduced as the ratio of the ionic conductivity of the SEI and that of the liquid electrolyte, where the latter is fixed to $1.5 \times 10^{-2} \text{ S cm}^{-1}$ at room temperature.^[30] To independently investigate the impact of the ionic conductivity of the artificial SEI it is first treated as an ideal elastomer. The flexibility of SEI is also critical mechanical property for metal anodes to address the issues of volume change during the electrochemical plating/stripping.^[31] In our model, only the elastic behavior of SEI is investigated in this work and the plastic deformation or stress relaxation of SEI is not included. The applied current density in this work was set as 0.5 mA cm^{-2} .

When the conductivity is very low, $\Gamma = 0.001$ – 0.01 in Figure 2a,b, there is a depletion of Li-ions in the SEI and as a result, the current density on the surface of the substrate is very low. With increasing conductivity, there is less Li-ion depletion in the SEI and the concentration gradient between the liquid electrolyte and the SEI is decreased, Figure 2a–c. Above $\Gamma = 0.1$ (Figure 2d and Figure S2a: Supporting Information) only negligible changes are observed with a high current density localized to the top of the pillars. The electrodeposited Li under the SEI with low ionic conductivity ($\Gamma = 0.001$ and 0.01) shows a teeth-like morphology and low electrodeposition probability during the whole process (Figure 2e,f), whereas at higher conductivities ($\Gamma \geq 0.1$) a bulb-like morphology and higher electrodeposition probability are found (Figure 2g,h and Figure S2b: Supporting Information). The above results indicate that $\Gamma = 0.1$ can be considered as a threshold value in order to obtain efficient and homogeneous electrodeposition of Li on a substrate covered with an artificial SEI, when considering the ionic conductivity alone.

To quantitatively analyze how the ionic conductivity of SEI affects the electrodeposition of Li, the distribution of Faradic current density on the substrate is calculated and shown in Figure 3 and Figure S3 (Supporting Information). The Faradic current density is close to zero when the ionic conductivity of the SEI is low, $\Gamma = 0.001$, but increases rapidly with increasing conductivity (Figure 3a and Figure S3a: Supporting Information). When the ionic conductivity of the SEI is above $\Gamma = 0.1$, the Faradic current density only shows little change at the initial state. As electrodeposition proceeds of Li the Faradic current density increases (Figure S3, Supporting Information). At the convergence state, it is concentrated to corners of the pillars when the SEI has a low low-ionic-conductivity ($\Gamma = 0.001$ and $\Gamma = 0.01$) but becomes more uniform when the ionic conductivity of SEI is over the threshold value $\Gamma > 0.1$ (Figure 3b). To confirm that $\Gamma > 0.1$ is a threshold value, simulations were run with SEIs with extremely high ionic conductivities, $\Gamma = 2.0$ – 10.0 , which has not been reported experimentally. As shown in Figure S4a–c (Supporting Information), an even distribution of Faradic current density is observed at such ultrahigh ionic conductivities. Here, the electric field lines go through, or even along, the SEI, suggesting that an ultrahigh ionic conductivity enables a freer transport of Li-ions. At the convergence state, the thickness of Li deposited on top of the pillars, as well as the curvature decreases with the increasing Γ (Figure S4d–f,

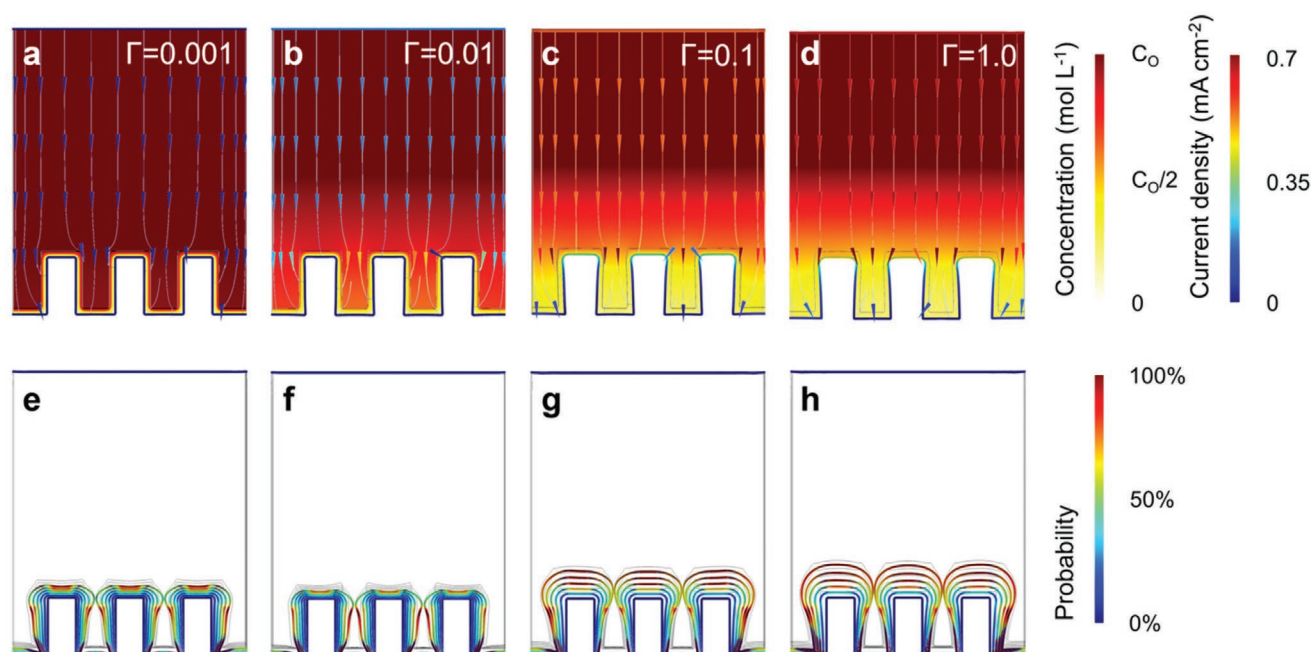


Figure 2. Electrodeposition of Li metal on substrates covered by SEIs with different ionic conductivities. Li-ion concentration (background color) and electric (colored arrows) fields at the initial state with substrates covered by SEIs with a) $\Gamma = 0.001$, b) $\Gamma = 0.01$, c) $\Gamma = 0.1$, d) and $\Gamma = 1.0$. Evolution of electrodeposition probability (colored profile lines) on substrates covered by SEIs with e) $\Gamma = 0.001$, f) $\Gamma = 0.01$, g) $\Gamma = 0.1$ and h) $\Gamma = 1.0$.

Supporting Information) and the electrodeposition probability is found to be uniform when Γ is above 5.0 (Figure S4g–i, Supporting Information).

As a result of Li deposition at the interface between an SEI with a finite Young's modulus and the substrate, local stress will be generated due to the deformation of the SEI, with a magnitude depending on the elastic modulus. To investigate the electrodeposition of Li including a stress field, the Young's modulus (E) of the SEI was set to 1 GPa. The results in Figure 4a–e show that the concentration gradient near the electrode surface decreases considerably, while Faradic current density is enhanced with increasing ionic conductivity in the region of $\Gamma = 0.001$ –1.0. This indicates an accelerated kinetics for the electrochemical reaction with increasing ionic conductivity in the SEI. The stress at the interface, induced by deposition of Li, varies over the surface of the pillars. As shown in Figure 4f,g and Figure S5a,b (Supporting Information), a stress concentration on the corners of the pillars is observed for electrodeposition under SEI with low ionic

conductivity ($\Gamma = 0.001$ and 0.01). With increasing ionic conductivity ($\Gamma = 0.1$ –1.0) the stress concentration region extends along the pillar and the magnitude of stress decreases (Figure 4h–j and Figure S5c–e: Supporting Information).

The deformation of the SEI and the resulting stress concentration will further affect the kinetics of Li electrodeposition. Statistics of von Mises stress, in form of vertical cross-sections starting from the boundary between substrate and SEI at the initial state, is shown in Figure 4k–o (Supporting Information). The boundary is marked by the white line and the corresponding coordinate for the starting point is 23 μm , as shown in Figure 4f–j (Supporting Information). The maxima of von Mises stress on the profile of pillar decreases with increasing ionic conductivity of the SEI film. These results suggest a compressed growth of Li in the vertical direction for the SEIs with low ionic conductivity ($\Gamma < 0.1$). A region of high-stress concentration is formed on the corner of the pillar where the SEI film has a high probability for cracking in the case of SEIs with moderate Young's modulus of 1 GPa.

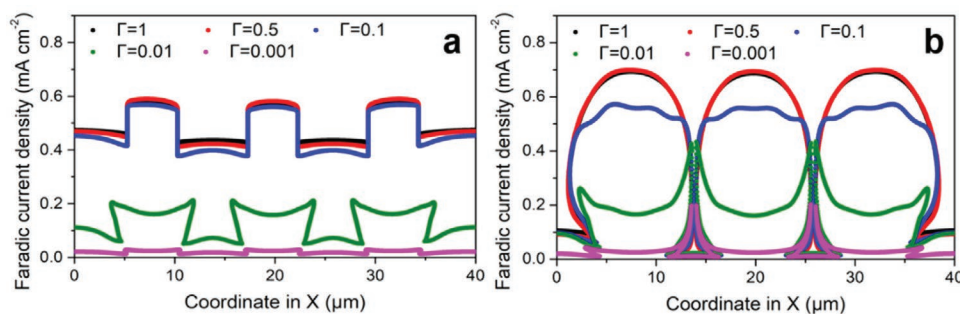


Figure 3. Distribution of Faradic current density on substrates covered by SEIs with various ionic conductivities at a) initial and b) convergence states.

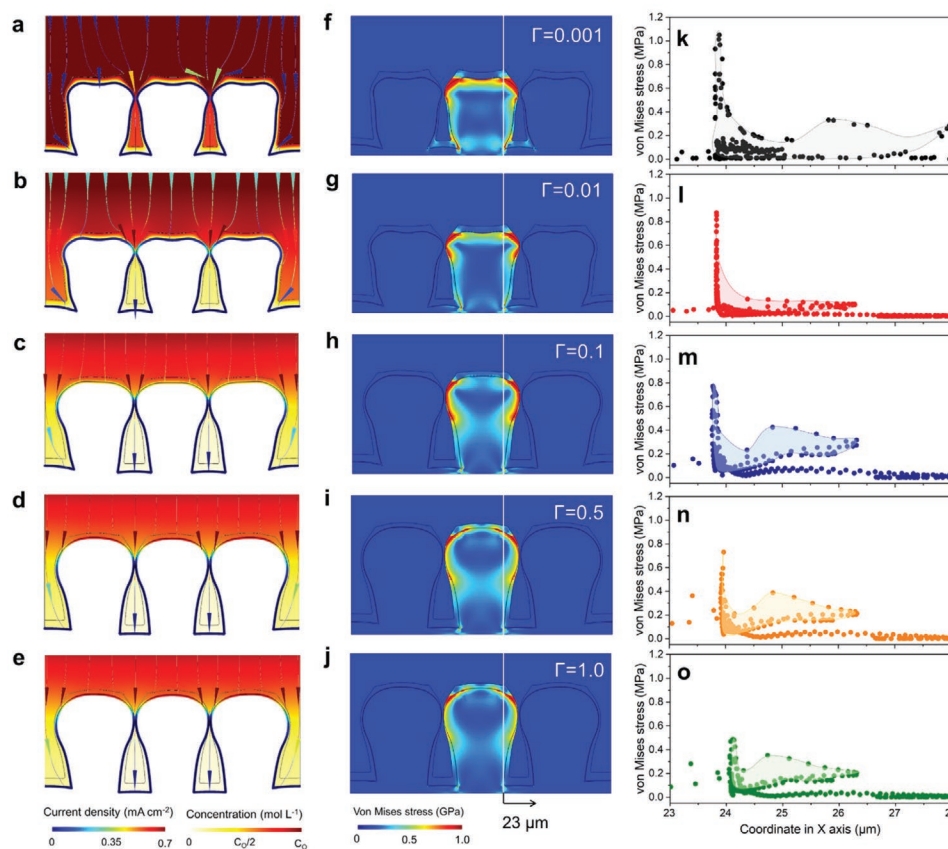


Figure 4. Electrodeposition of Li metal on substrates covered by SEIs with fixed Young's modulus and different ionic conductivities. Concentration (background color) and electric (colored lines) fields near substrates covered by SEIs with $E = 1$ GPa and a) $\Gamma = 0.001$, b) $\Gamma = 0.01$, c) $\Gamma = 0.1$, d) $\Gamma = 0.5$ and e) $\Gamma = 1.0$. Stress field at Li-SEI interface with different ionic conductivity of SEI f) $\Gamma = 0.001$, g) $\Gamma = 0.01$, h) $\Gamma = 0.1$, i) $\Gamma = 0.5$ and j) $\Gamma = 1.0$. Von Mises stress at Li-SEI interface with different ionic conductivity of SEI k) $\Gamma = 0.001$, l) $\Gamma = 0.01$, m) $\Gamma = 0.1$, n) $\Gamma = 0.5$ and o) $\Gamma = 1.0$. The starting point at the x-axis ($23 \mu\text{m}$) is the boundary between substrate and SEI at the foot of the pillar at the initial state, shown in Figure S1 (Supporting Information).

To investigate the effect of mechanical strength the Young's modulus of the SEI was varied, $E = 0.1$ – 100 GPa, while the ionic conductivity was fixed to $\Gamma = 0.1$. The evolution of the morphology in Figure 5a,b and Figure S6 (Supporting Information) shows that a preferred growth is observed at the corners of the pillars of the substrate when the Young's modulus is lower than 3.0 GPa. This trend is also shown by the current density at (see in Figure 5f–j, Supporting Information). A preferred growth at some locations will invariably induce stress concentration. As shown in Figure 5k,l, a significant stress concentration is revealed for low Young's modulus ($E = 0.5$ and 0.1 GPa) in the neck region of the teeth-like morphology of deposited Li on the pillars of the substrate. This induces a significant risk of breakdown of deposited Li layer. With increased mechanical strength of the SEI ($E = 1.0$ – 3.0 GPa), the morphology of deposited Li changes to bulb-like and the region of stress concentration moves to the top corners of the pillars on the substrate (Figure 5m,o). For SEIs with a very high mechanical strength, $E > 4.0$ GPa, a uniform stress distribution, with very little stress concentration is observed (Figure S7, Supporting Information), as a result of a much more even Li electrodeposition. From the distribution of von Mises, Figure S8 (Supporting Information), a decrease in the maximum stress and a shift of the region of stress concentration toward the center of the pillars is found for

increasing Young's modulus of the SEI. Therefore, increased mechanical strength of the SEI is an effective way to suppress stress concentration and to reduce the possibility of breaking the SEI, or even the whole electrode, during electrodeposition. However, 4.0 GPa can be considered as a threshold value since there is little change when increasing the strength beyond this value.

The effect of Young's modulus of the SEI is further investigated by quantitatively analyzing the deformation of electrodeposited Li along the horizontal (X) and vertical (Y) directions. The deformation ratio (deformation in Y divided by deformation in X) in Figure 6a shows a double logarithmic behavior with Young's modulus, illustrating that the enhanced compression in the vertical direction switches to the horizontal direction as the strength of the SEI increases, with $E \approx 4$ GPa as a critical value for this transition. Furthermore, maximum thicknesses of Li in the horizontal and vertical directions were derived from the convergence states in Figure 5 and Figures S6 and S7 (Supporting Information). A preferred vertical growth is found for $E < 4$ GPa whereas as uniform growth is obtained for higher Young's modulus of the SEI, also shown uniformity index for electrodeposition, Figure S9 (Supporting Information). However, if the SEI is very rigid ($E \geq 5.0$ GPa) this will suppress the overall growth rate of Li due to lower Faradaic current density, thus resulting in less efficient Li-plating, with

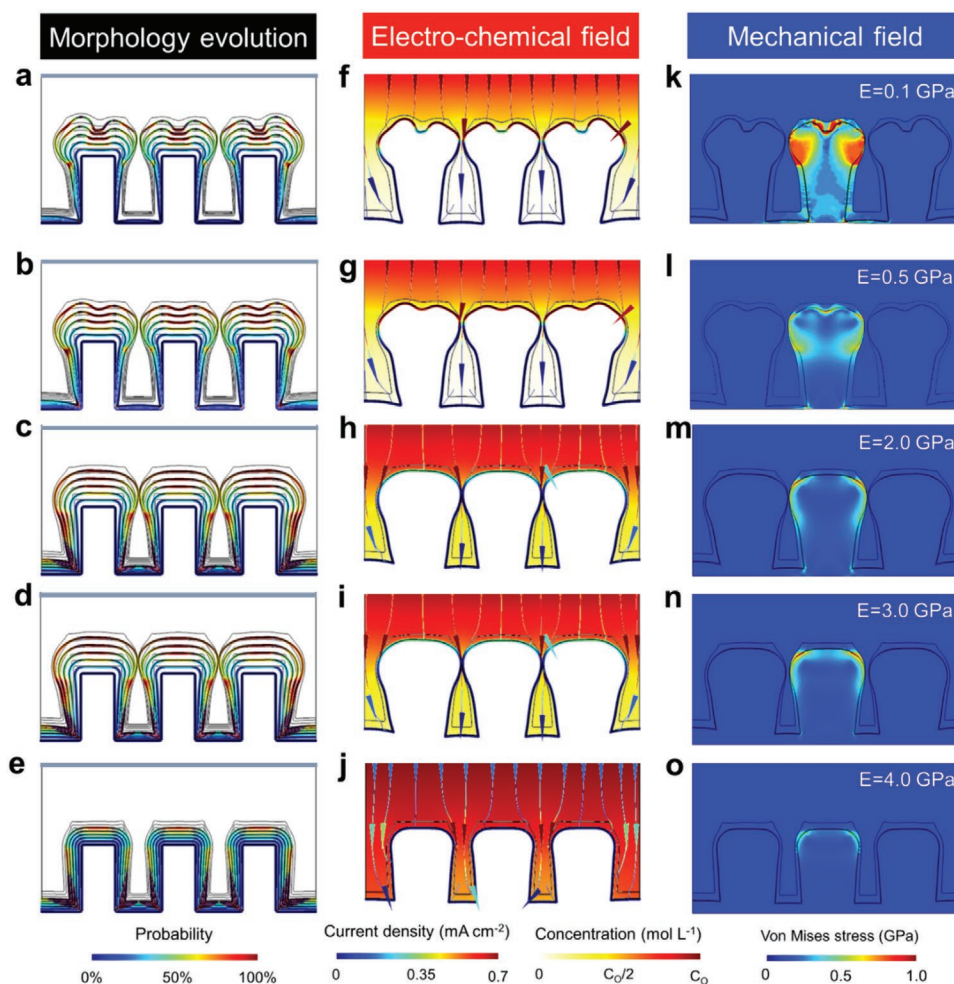


Figure 5. Morphology evolution and distribution of physical fields on electrodeposited Li covered by SEI with different mechanical strength. Evolution of electrodeposition probability (colored profile lines) on substrates covered by SEIs with Young's modulus a) $E = 0.1$ GPa, b) $E = 0.5$ GPa, c) $E = 2.0$ GPa, d) $E = 3.0$ GPa, e) $E = 4.0$ GPa. Concentration (background color) and electric (colored lines) fields near substrates covered by SEIs with Young's modulus f) $E = 0.1$ GPa, g) $E = 0.5$ GPa, h) $E = 2.0$ GPa, i) $E = 3.0$ GPa, j) $E = 5.0$ GPa at convergence state. Stress field obtained with SEIs with different Young's modulus k) $E = 0.1$ GPa, l) $E = 0.5$ GPa, m) $E = 2.0$ GPa, n) $E = 3.0$ GPa, o) $E = 4.0$ GPa at convergence state.

the time to convergence state, Figure 6c, increasing exponentially with the Young's modulus. Therefore, a moderate Young's modulus around 4.0 GPa is a good compromise to mitigate stress concentration in order to suppress the breakdown of

the SEI and to promote uniform electrodeposition without decreasing the deposition rate significantly.

To compare our modeling results to experimental data, ionic conductivity and Young's modulus of artificial SEI con-

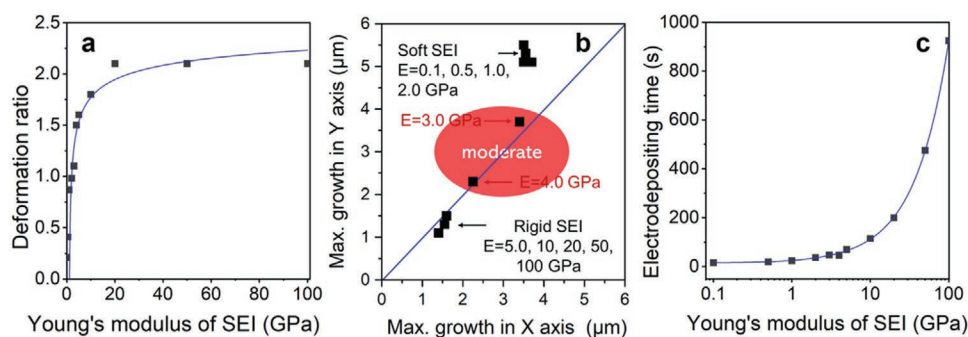


Figure 6. Uniformity of Li electrodeposition with different mechanical strengths of the SEI. a) Deformation ratio of electrodeposited Li (see text) as a function of Young's modulus at convergence state. b) Max growth of Li in horizontal (X) and vertical (Y) directions. c) Electrodeposition time as a function of Young's modulus of SEI. Symbols are modeling data and full lines are fits to double logarithmic (a), and exponential functions (c).

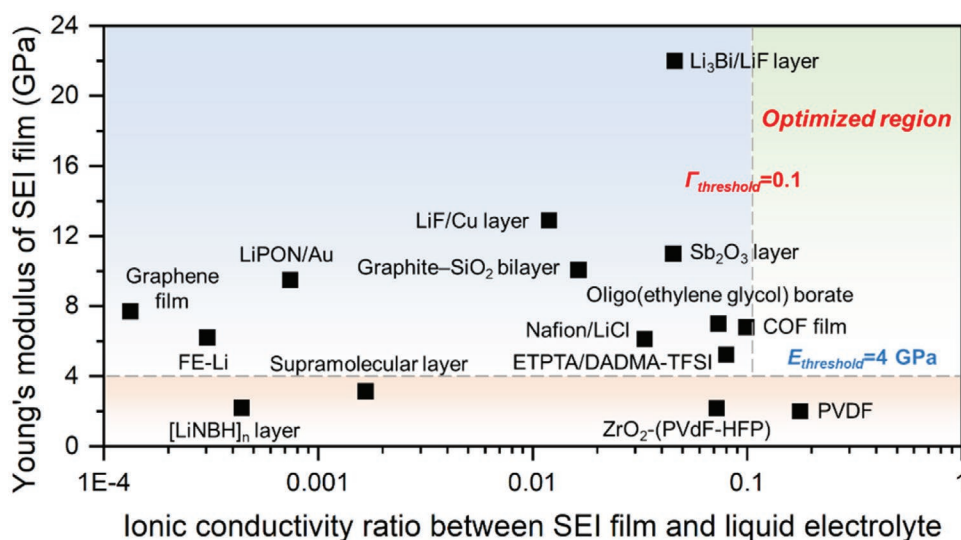


Figure 7. Design guidelines for artificial SEIs to promote uniform electrodeposition. Comparison of Young's modulus and ionic conductivity for artificial SEI concepts reported in literature, details and references found in Table S2 (Supporting Information). Threshold values for ionic conductivity and mechanical strength are marked by the transition from blue to red and green to blue regions.

cepts reported in literature are listed in Table S2 (Supporting Information) and plotted in **Figure 7**. It is interesting to note that most of the reported concepts have lower ionic conductivity than the threshold value $\Gamma = 0.1$ identified in our work. This implies that a homogenous electrodeposition with these SEIs will be difficult to achieve at high current densities or low temperature when Li-ion depletion is enhanced.^[5b] From the mechanical point of view, the reported artificial SEI concepts can be sorted into two regions, those with a Young's modulus above and below $E = 4.0$ GPa. Most of the concepts are based on materials with relatively high mechanical strength, $E \geq 4.0$ GPa, which is enough to realize uniform growth of Li if the ionic conductivity is high enough. However, a high ion conductivity is most often found for soft SEIs, which induces a promoted growth in the vertical direction, following the results in our work, with an increased risk of mechanical failure of the SEI or even the electrode. The comparison of our modelling work to results reported in literature clearly points to that a significant advancement on improving the ionic conductivity of artificial SEIs while keeping the high mechanical strength is the most important direction of future work.

3. Conclusion

We report on an electro-chem-mechanical model based on the modified Butler–Volmer equation and its implementation in phase-field modeling to establish the correlation between physical properties of artificial SEIs and electrodeposition behavior of Li. Our simulation results show that both ionic conductivity and mechanical strength of SEI determine the distribution of stress at the interface as well as the local deposition rate. The electrodeposition of Li under SEI with low ionic conductivity results in a highly localized deposition stress concentration at these points. The stress concentration will not only control the kinetics of the electrochemical reaction but also induce the risk of mechanical failure of the SEI. An enhanced mechanical

strength of the SEI can on the other hand mitigate stress concentration and a uniform distribution of von Mises stress and electrodeposition rate at the interface between the SEI and the Li-metal is obtained when the Young's modulus of SEI is greater than a threshold of 4.0 GPa. In our work we identify critical values of ionic conductivity and mechanical strength of the artificial SEI to enable uniform electrodeposition of Li. A comparison of our modelling results with previously reported experimental results clearly identifies that improving the ionic conductivity, without compromising the mechanical strength, of artificial SEIs is the key development direction to promote uniform of deposited Li. Furthermore, the methodology applied here for Li-deposition can be directly transferred to investigate the electro-chemo-mechanical coupling mechanism at the interface between liquid/solid electrolytes and other active metal electrodes, which will boost the practical application of metal anodes in next-generation batteries.

Supporting Information

Supporting Information is available from the Wiley Online Library or from the author.

Acknowledgements

Y.L. and X.X. contributed equally to this work. The authors thank for the support from Chalmers Areas of Advance Materials Science and Energy. This work was financially supported by the National Natural Science Foundation of China (No. 51802256) and China Scholarship Council (No. 201908090043). O.O.K. gratefully acknowledges the financial support from the Ministry of Science and Higher Education of the Russian Federation (Agreement No. 075-15-2021-606).

Conflict of Interest

The authors declare no conflict of interest.

Data Availability Statement

The data that support the findings of this study are available from the corresponding author upon reasonable request.

Keywords

artificial SEI, electro-chemo-mechanical models, electrodeposition, Li metal anodes, phase-field modeling

Received: November 15, 2021

Revised: December 21, 2021

Published online:

- [1] a) Y. Lu, C. Z. Zhao, H. Yuan, X. B. Cheng, J. Q. Huang, Q. Zhang, *Adv. Funct. Mater.* **2021**, 31, 2009925; b) H. Li, *Joule* **2019**, 3, 911; c) J. Xiao, Q. Y. Li, Y. J. Bi, M. Cai, B. Dunn, T. Glossmann, J. Liu, T. Osaka, R. Sugiura, B. B. Wu, J. H. Yang, J. G. Zhang, M. S. Whittingham, *Nat. Energy* **2020**, 5, 561.
- [2] a) M. T. McDowell, F. J. Q. Cortes, A. C. Thenuwara, J. A. Lewis, *Chem. Mater.* **2020**, 32, 8755; b) X. Zhang, Y. Yang, Z. Zhou, *Chem. Soc. Rev.* **2020**, 49, 3040.
- [3] a) B. Liu, J.-G. Zhang, W. Xu, *Joule* **2018**, 2, 833; b) P. Albertus, S. Babinec, S. Litzelman, A. Newman, *Nat. Energy* **2017**, 3, 16; c) Y. Liu, S. Xiong, J. Wang, X. Jiao, S. Li, C. Zhang, Z. Song, J. Song, *Energy Storage Mater.* **2019**, 19, 24.
- [4] a) S. S. Zhang, *ACS Appl. Energy Mater.* **2018**, 1, 910; b) S. H. Yu, X. Huang, J. D. Brock, H. D. Abruna, *J. Am. Chem. Soc.* **2019**, 141, 8441; c) H. Sano, H. Sakaebe, H. Senoh, H. Matsumoto, *J. Electrochem. Soc.* **2014**, 161, A1236; d) K. N. Wood, E. Kazyak, A. F. Chadwick, K. H. Chen, J. G. Zhang, K. Thornton, N. P. Dasgupta, *ACS Cent. Sci.* **2016**, 2, 790; e) F. Sun, C. Yang, I. Manke, L. Chen, S. Dong, *Mater. Today* **2020**, 38, 7; f) X. Shen, R. Zhang, P. Shi, X. Chen, Q. Zhang, *Adv. Energy Mater.* **2021**, 11, 2003416.
- [5] a) Y. Liu, X. Xu, M. Sadd, O. O. Kapitanova, V. A. Krivchenko, J. Ban, J. Wang, X. Jiao, Z. Song, J. Song, S. Xiong, A. Matic, *Adv. Sci.* **2021**, 8, 2003301; b) X. Xu, Y. Liu, J. Y. Hwang, O. O. Kapitanova, Z. Song, Y. K. Sun, A. Matic, S. Xiong, *Adv. Energy Mater.* **2020**, 10, 2002390; c) X. Ai, *Energy Storage Sci. Technol.* **2018**, 7, 37; d) J. Xiao, *Science* **2019**, 366, 426.
- [6] K. Tasaki, K. Kanda, S. Nakamura, M. Ue, *J. Electrochem. Soc.* **2003**, 150, A1628.
- [7] a) S. Shi, P. Lu, Z. Liu, Y. Qi, L. G. Hector Jr., H. Li, S. J. Harris, *J. Am. Chem. Soc.* **2012**, 134, 15476; b) J. G. Thevenin, R. H. Muller, *J. Electrochem. Soc.* **1987**, 134, 273; c) D. Aurbach, M. L. Daroux, P. W. Faguy, E. Yeager, *J. Electrochem. Soc.* **1987**, 135, 1863.
- [8] a) C. Yan, X. B. Cheng, Y. Tian, X. Chen, X. Q. Zhang, W. J. Li, J. Q. Huang, Q. Zhang, *Adv. Mater.* **2018**, 30, 1707629; b) C. Yan, X. B. Cheng, Y. X. Yao, X. Shen, B. Q. Li, W. J. Li, R. Zhang, J. Q. Huang, H. Li, Q. Zhang, *Adv. Mater.* **2018**, 30, 1804461.
- [9] Y. Y. Liu, X. Y. Xu, X. X. Jiao, L. N. Guo, Z. X. Song, S. Z. Xiong, J. X. Song, *Chem. Eng. J.* **2019**, 371, 294.
- [10] X. B. Cheng, R. Zhang, C. Z. Zhao, F. Wei, J. G. Zhang, Q. Zhang, *Adv. Sci.* **2016**, 3, 1500213.
- [11] a) A. Mistry, C. Fear, R. Carter, C. T. Love, P. P. Mukherjee, *ACS Energy Lett.* **2018**, 4, 156; b) J.-Y. Hwang, S.-J. Park, C. S. Yoon, Y.-K. Sun, *Energy Environ. Sci.* **2019**, 12, 2174; c) L. Xiang, X. Ou, X. Wang, Z. Zhou, X. Li, Y. Tang, *Angew. Chem., Int. Ed. Engl.* **2020**, 59, 17924; d) Y. Yu, G. Huang, J.-Y. Du, J.-Z. Wang, Y. Wang, Z.-J. Wu, X.-B. Zhang, *Energy Environ. Sci.* **2020**, 13, 3075; e) J. Wang, G. Huang, K. Chen, X. B. Zhang, *Angew. Chem., Int. Ed. Engl.* **2019**, 131, 18408; f) J. Wang, G. Huang, J. M. Yan, J. L. Ma, T. Liu, M. M. Shi, Y. Yu, M. M. Zhang, J. L. Tang, X. B. Zhang, *Natl. Sci. Rev.* **2021**, 8, nwa150; g) T. Liu, Y. Yu, X.-Y. Yang, J. Wang, X.-B. Zhang, *Small Struct.* **2020**, 1, 2000015.
- [12] a) Y. Sakurai, A. Sakuda, A. Hayashi, M. Tatsumisago, *Solid State Ionics* **2011**, 182, 59; b) Y. J. Zhang, X. Y. Liu, W. Q. Bai, H. Tang, S. J. Shi, X. L. Wang, C. D. Gu, J. P. Tu, *J. Power Sources* **2014**, 266, 43; c) E. Kazyak, K. N. Wood, N. P. Dasgupta, *Chem. Mater.* **2015**, 27, 6457.
- [13] a) N. W. Li, Y. X. Yin, C. P. Yang, Y. G. Guo, *Adv. Mater.* **2016**, 28, 1853; b) S. Liu, X. Xia, S. Deng, D. Xie, Z. Yao, L. Zhang, S. Zhang, X. Wang, J. Tu, *Adv. Mater.* **2019**, 31, 1806470; c) H. Chen, A. Pei, D. Lin, J. Xie, A. Yang, J. Xu, K. Lin, J. Wang, H. Wang, F. Shi, D. Boyle, Y. Cui, *Adv. Energy Mater.* **2019**, 9, 1900858; d) Y. Gao, T. Rojas, K. Wang, S. Liu, D. W. Wang, T. H. Chen, H. Y. Wang, A. T. Ngo, D. H. Wang, *Nat. Energy* **2020**, 5, 534; e) Y. Yu, G. Huang, J. Z. Wang, K. Li, J. L. Ma, X. B. Zhang, *Adv. Mater.* **2020**, 32, 2004157; f) T. Liu, X. L. Feng, X. Jin, M. Z. Shao, Y. T. Su, Y. Zhang, X. B. Zhang, *Angew. Chem., Int. Ed. Engl.* **2019**, 58, 18240.
- [14] a) J. Xie, L. Liao, Y. Gong, Y. Li, F. Shi, A. Pei, J. Sun, R. Zhang, B. Kong, R. Subbaraman, J. Christensen, Y. Cui, *Sci. Adv.* **2017**, 3, ea03170; b) E. Cha, M. D. Patel, J. Park, J. Hwang, V. Prasad, K. Cho, W. Choi, *Nat. Nanotechnol.* **2018**, 13, 337; c) Y. Gao, Z. Yan, J. L. Gray, X. He, D. Wang, T. Chen, Q. Huang, Y. C. Li, H. Wang, S. H. Kim, T. E. Mallouk, D. Wang, *Nat. Mater.* **2019**, 18, 384; d) Y. Gao, Y. Zhao, Y. C. Li, Q. Huang, T. E. Mallouk, D. Wang, *J. Am. Chem. Soc.* **2017**, 139, 15288; e) K. Liu, A. Pei, H. R. Lee, B. Kong, N. Liu, D. Lin, Y. Liu, C. Liu, P. C. Hsu, Z. Bao, Y. Cui, *J. Am. Chem. Soc.* **2017**, 139, 4815.
- [15] a) A. R. Despic, J. Diggel, J. O. M. Bockris, *J. Electrochem. Soc.* **1968**, 115, 507; b) G. Yoon, S. Moon, G. Ceder, K. Kang, *Chem. Mater.* **2018**, 30, 6769; c) R. Zhang, X. Shen, X.-B. Cheng, Q. Zhang, *Energy Storage Mater.* **2019**, 23, 556.
- [16] a) J.-N. Chazalviel, *Phys. Rev. A* **1990**, 42, 7355; b) C. Brissot, M. Rosso, J. N. Chazalviel, P. Baudry, S. Lascaud, *Electrochim. Acta* **1998**, 43, 1569.
- [17] Z. Hong, V. Viswanathan, *ACS Energy Lett.* **2018**, 3, 1737.
- [18] A. Ferrese, J. Newman, *J. Electrochem. Soc.* **2014**, 161, A1350.
- [19] P. Liu, Y. Wang, H. Hao, S. Basu, X. Feng, Y. Xu, J. A. Boscoboinik, J. Nanda, J. Watt, D. Mitlin, *Adv. Mater.* **2020**, 32, 2002908.
- [20] Y. Liu, Y. Zhai, Y. Xia, W. Li, D. Zhao, *Small Struct.* **2021**, 2, 2000118.
- [21] H. J. Ploehn, P. Ramadass, R. E. White, *J. Electrochem. Soc.* **2004**, 151, A456.
- [22] L. Chen, H. W. Zhang, L. Y. Liang, Z. Liu, Y. Qi, P. Lu, J. Chen, L.-Q. Chen, *J. Power Sources* **2015**, 300, 376.
- [23] a) D. Grazioli, V. Zadin, D. Brandell, A. Simone, *Electrochim. Acta* **2019**, 296, 1142; b) A. V. Sokirko, F. H. Bark, *Electrochim. Acta* **1995**, 40, 1983.
- [24] A. Einstein, *Ann. Phys. (in German)* **1905**, 322, 549.
- [25] a) A. Jana, S. I. Woo, K. S. N. Vikrant, R. E. García, *Energy Environ. Sci.* **2019**, 12, 3595; b) Y. Lee, B. Ma, P. Bai, *Energy Environ. Sci.* **2020**, 13, 3504.
- [26] a) P. Barai, K. Higa, V. Srinivasan, *Phys. Chem. Chem. Phys.* **2017**, 19, 20493; b) C. Monroe, J. Newman, *J. Electrochem. Soc.* **2005**, 152, A396.
- [27] C. Monroe, J. Newman, *J. Electrochem. Soc.* **2004**, 151, A880.
- [28] L. Gao, Z. Guo, *Comput. Mater. Sci.* **2020**, 183, 109919.
- [29] J. Rychlewski, *J. Appl. Math. Mech. (Engl. Transl.)* **1984**, 48, 303.
- [30] L. Gireaud, S. Grugeon, S. Laruelle, B. Yrieix, J. M. Tarascon, *Electrochem. Commun.* **2006**, 8, 1639.
- [31] J. L. Ma, F. L. Meng, Y. Yu, D. P. Liu, J. M. Yan, Y. Zhang, X. B. Zhang, Q. Jiang, *Nat. Chem.* **2019**, 11, 64.